MICROMAGNETIC SUSCEPTOMETER FOR THE MEASUREMENT OF THE MAGNETIC SUSCEPTIBILITY OF THE ACTINIDES

A Dissertation

Presented for the

Doctor of Philosophy

Degree

The University of Tennessee, Knoxville

Stanley Eugene Nave

August 1979

DISCLAIMER

DOE/ER/10348--3

MASTER

ACKNOWLEDGMENTS

The author is extremely grateful to Dr. P. G. Huray who has given invaluable guidance and moral support during the course of this work. The author also acknowledges much helpful advice from Drs. J. R. Thompson, J. O. Thomson, and Joseph Peterson. Special thanks go to Dr. Daniel A. Damien for preparing the curium metal samples.

Appreciation is extended to the University of Tennessee for a teaching assistantship and to the University and Drs. Joseph Peterson and P. G. Huray for research assistantships. Thanks are also given to the Oak Ridge Associated Universities (ORAU) for a research fellowship as part of the Laboratory Graduate Participation program administered by ORAU for the U.S. Department of Energy. The author also expresses gratitude to the Oak Ridge National Laboratory (operated for the U.S. Department of Energy under Contract W-7405-eng-26 with the Union Carbide Corporation) and to the Transuranium Research Laboratory for use of their facilities.

The author also wishes to express thanks to the excellent technical staff at the Transuranium Research Laboratory. In particular the author acknowledges the assistance of John A. Burkhalter, T. C. Minton, Earnest L. Early, Albert L. Massey, Kyle E. Sowder, Jim Tarrant, William D. Carden, Terry Collins, Charles E. Haynes, and Jim E. Smith.

The author could not have made it without the moral support of his wife Kathi through the many trying times. Also undying gratitude is given for the support of his parents Lloyd E. and Selma Nave during the author's educational career.

ABSTRACT

A device with the sensitivity for measuring the magnetic susceptibility of small volume samples (10^{-7} cm^3) as a function of temperature from 4.2K to 300K is described as designed specifically for measurements with microgram or submicrogram quantities of the actinide metals. Specifically, results are given for the susceptibility of curium-248 in the temperature range from 4.2K to 300K.

The susceptometer is calibrated with a 71 microgram sphere of lead. From this measurement and the measurements with curium the minimum measureable volume susceptibility for a one microgram, metal sample is determined to be 7.4×10^{-8} (CGS). The temperature of the sample is determined by measuring simultaneously the susceptibility of a sample of Gd_2O_3 in thermal contact with the curium. The magnetic field is measured using the critical field of the lead as a calibrating point. The Gd_2O_3 signal is used as the measure for fields.

For a 41.2 microgram sample of curium-248, measurements were made in fields of .45G and 20.9G. There is evidence for two magnetic transitions. One in the range 77-78K is clearly an antiferromagnetic to paramagnetic transition. The other occurs in the range 187-206K and resembles this type of transition also.

TABLE OF CONTENTS

CHAPTER		PAGE
I.	INTRODUCTION	1
	Difficulties Posed by the Actinides	1
	Results Expected for the Actinides	4
	Curium as a Sample	5
II.	THEORY OF ACTINIDE METALS	6
	Introduction	6
	Susceptibility Using L-S Coupling Model	6
	Breakdown of L-S Coupling	8
III.	MICROMAGNETIC SUSCEPTOMETER	11
	Overview of the System	11
	Flux Measurement	15
	Second Derivative Coil Design	18
	Shield and Flux-Trapping Tube	19
	Superconducting Magnet	24
	Coil Holder	24
	Data Acquisition	26
IV.	SAMPLE HOLDER	31
	Construction	31
	Magnetic Measurements on an Empty Holder	31
	Weighing and Loading of Samples	32
V.	DETERMINING THE SUSCEPTIBILITY FROM THE DATA	34
	Flux vs. Position Function	34
	Computer Fitting of Data	36
	Determination of Susceptibility	37
	Deconvolution	42
VI.	CALIBRATION OF THE SUSCEPTOMETER WITH A LEAD SPHERE	45
	Demagnetizing Factor	45
	Preparation of Spheres	46
	Sphericity	46
	Determination of the Magnetic Field with the Sphere	48

CHAPTER PAGE

VII. THERMOMETRY 49

Copper-Constantan Thermocouple 49
Gd_2O_3: A Magnetic Thermometer 50

VIII. RESULTS AND DISCUSSION 53

Sensitivity 53
Reproducibility and Accuracy 54
Preliminary Determination of Curium Susceptibility . . . 55
Conclusion 59

REFERENCES 61

VITA 64

LIST OF TABLES

TABLE		PAGE
I.	Properties of Selected Transuranium Nuclides	2
II.	Comparison of Measured Coil Dimensions and Those Determined by Computer Fit to Data	38
III.	Results of Cm 41278 Spark Source Mass Spectrolysis	60

LIST OF FIGURES

FIGURE		PAGE
1.	Overview of Susceptometer	12
2.	Sample Holder Configuration	13
3.	Detail of Low Temperature Part of Susceptometer	14
4.	Cross Section of SQUID and Flux-Transformer	16
5.	Second Derivative Coils and Flux-Trapping Tube	20
6.	Diagram Illustrating the Zero Order Approximation to the Image Problem	23
7.	Flux Profiles at 4.2K and 12.8K	27
8.	Data Acquisition System	28
9.	Computer Fit to the Sample Flux Profile	39
10.	A Plot of the Difference between the Data of Figure 9 and a Computer Fit with the Off-Axis Distance Fixed at Zero	40
11.	A Plot of the Theoretical Off-Axis Term for the Flux as a Function of Position for an Off-Axis Distance of .3 mm	41
12.	Deconvoluted Lead, Gd_2O_3 Flux Profiles	44
13.	A Plot of the Lead Magnetic Moment vs. Gd_2O_3 Moment as the Field is Varied from 0G to 600G	47
14.	A Plot of the Inverse of the Peak-to-Peak Flux of the Gd_2O_3 Sample vs. Temperature	51
15.	Susceptibility vs. Temperature for a 41.2 μgram Cm^{248} Sample at .45G	56
16.	Susceptibility vs. Temperature for a 41.2 μgram Cm^{248} Sample at 20.9G	57

CHAPTER I

INTRODUCTION

A. DIFFICULTIES POSED BY THE ACTINIDES

The discovery of the transuranium elements (elements 93-103) has presented a new and difficult challenge to the scientific community. Progress with these elements has required work on the frontier of experimental techniques as well as the application of new theoretical ideas. The elements beyond curium in the periodic table are currently available for susceptibility measurements only in microgram quantities, and their specific radioactivity (as indicated in Table I) precludes the use of larger quantities for health and safety reasons. Micro-techniques are therefore necessary for handling these samples. The safety factor complicates the matter by requiring one to work in glove boxes and to incorporate multiple containment techniques into the design of any experimental equipment. For this reason our variable temperature (4.2K to 300K) magnetic susceptometer was designed specifically to maximize sensitivity to the magnetic flux produced by small volume samples. Design features of several high sensitivity large sample magnetic susceptometers[1,2,3] were adapted with this goal in mind. These susceptometers are based upon superconductive flux sensors which measure the magnetic flux through a set of coils due to a sample magnetized in a uniform field. They have sensitivities several orders of magnitude better than the mechanical balance type of

TABLE I

PROPERTIES OF SELECTED TRANSURANIUM NUCLIDES[a]

Nuclide	Half-Life	Energies of Principle Emissions (MeV) α	β	Specific Activity (Ci/g)
^{244}Cm	18.099y	5.81		80.94
^{248}Cm	3.397×10^{5}y	5.05		4.24×10^{-3}
^{249}Bk	314d	5.4	.125	1.67×10^{3}
^{249}Cf	352y	5.81		4.08
^{253}Es	20.467d	6.62		2.52×10^{4}

[a]Oak Ridge National Laboratory Report ORNL-5034.

susceptometers, such as Faraday devices,[4] which are based upon a measurement of the force on a magnetized sample in a nonuniform field. It was hoped to preserve the sensitivity of these large sample susceptometers, which are designed for typical sample volumes of 10^{-1} cm^3, by scaling down the size of the flux sensing coils in accord with the sample dimensions, which are on the order of 10^{-7} cm^3, and thus to create a microsusceptometer. A minimum measurable volume susceptibility of 7.5×10^{-8} (CGS) for a 1 microgram sample of curium has been achieved. This represents an increase of two orders of magnitude over Faraday devices designed for microgram metallic samples.[5]

The theorist also has a very complicated system to treat in the actinides. Even though they are similar to the rare earths (the actinides involve a filling of an atomic 5f electronic state while the rare earths involve filling a 4f state) the actinides are much more complicated to treat in the metallic state due to the greater spatial extent of the 5f wavefunction and a larger contribution from relativistic effects. The rare earth metals are not appreciably different from rare earth ions in their high temperature magnetic behavior due to the small spatial extent of the wavefunction. They have been treated successfully theoretically (with excellent experimental agreement) using ionic states in which J, L, and S (the total, orbital, and spin angular momenta respectively) are good quantum numbers and a ground state derived from Hund's rule (maximum S and maximum L consistent with maximum S). Even the theory of the low temperature magnetic behavior of the rare earth metals is well

developed. In this region, where magnetic ordering and spin waves[6] are important, the results are usually explained by spin-spin interactions between ionic cores due to long-range oscillations in the spin of the conduction electron sea. This is known as the Ruderman-Kittel-Kasuya-Yosida effect (RKKY oscillations). The metallic actinide behavior is complicated in both temperature regions by the greater spatial extent of the 5f wavefunction. Overlap of wavefunctions from neighboring sites leads to direct exchange interactions and hybridization of the f, d, and s atomic states. It does appear, however, that the actinide wavefunctions become more localized with increasing atomic number and one expects the metallic actinide behavior to approach that of its rare earth counterpart for elements with z above 95 in the chemical series. For the heavier actinides, however, Russell-Saunders coupling,[7] which is assumed for the rare earths, breaks down and there is a pronounced tendency toward j-j coupling.[8]

B. RESULTS EXPECTED FOR THE ACTINIDES

From susceptibility measurements we desire information concerning the degree of localization versus hybridization of the 5f electronic state in the heavy actinide metals. This can be determined from the effective localized magnetic moment in the temperature range above all magnetic transitions. A lowering of this value from the atomic value can be interpreted in terms of hybridization. The type of magnetic ordering at low temperatures—if any—is also of interest since spin wave structures exist for the rare earth counterparts to the actinide metals. This microsusceptometer makes possible these determinations.

C. CURIUM AS A SAMPLE

The curium-248 used for this work was produced as part of the heavy element program of the Transuranium Research Laboratory at the Oak Ridge National Laboratory. The curium was obtained by intense neutron irradiation of a suitable uranium target in a high flux isotope reactor (HFIR). The curium-248 is obtained by allowing Cf-252 to decay. The curium is then separated from the californium and extensively purified.[9] Previous work has been done using the more radioactive isotope curium-244.[10] We felt that it was important to repeat these measurements on curium-248 to determine any effects due to self-irradiation damage from the alpha decay particles. Due to the increased sensitivity, the susceptometer is designed for work in smaller magnetic fields (0.5 → 2000G) than were used for the previous measurements (3.5-15KG) on curium opening up a new area of investigation.

CHAPTER II

THEORY OF ACTINIDE METALS

A. INTRODUCTION

The electronic structure of the actinide series is characterized by a filling of the 5f atomic state. It is the general concensus that the magnetic behavior of the heavy actinides, i.e., those after americium in the periodic table, may be described by a perturbation of their rare earth counterparts which are characterized by a filling of the atomic 4f state. The perturbation is brought about by a breakdown of the pure Russell-Saunders coupling scheme which, when used in a susceptibility calculation for the rare earths, gives excellent agreement with experiment. For the actinides there is a pronounced tendency towards j-j coupling. Evidence of j-j coupling is found in the spin-orbital coupling parameters for the actinides measured by Carnall and Wybourne.[11] They found parameters approximately twice as large as those of the corresponding lanthanide.

B. SUSCEPTIBILITY USING L-S COUPLING MODEL

Van Vleck[12] has derived a formula for the case of Russell-Saunders coupling. He has shown that, for a state in which J is a good quantum number, the susceptibility is given by:

$$\chi = N\mu_B^2 \frac{\sum_J \{[g_J^2 J(J+1)/3kT] + \alpha_J\}(2J+1)e^{-W_J^0/kT}}{\sum_J (2J+1)e^{-W_J^0/kT}}, \quad (1)$$

where W_J^0 = energy of J^0 state,

N = atomic density,

$$g_J = 1 + \frac{S(S+1) + J(J+1) - L(L+1)}{2J(J+1)},$$

k = Boltzmann's constant,

μ_B = the Bohr magneton

$$\alpha_J = \frac{1}{6(2J+1)} \left[\frac{F(J+1)}{h\nu(J+1;J)} - \frac{F(J)}{h\nu(J;J-1)}\right]$$

$$F(J) = \frac{1}{J} [(S+L+1)^2 - J^2][J^2 - (S-L)^2].$$

There are two approximations of this formula depending on the size of the multiplet intervals compared to kT:

(1) For $kT >> W_J^0$:

$$\chi = \frac{N\mu_B^2}{3kT} [4S(S+1) + L(L+1)] . \quad (2)$$

This corresponds to the breakdown of L-S coupling at high temperatures.

(2) For $kT << W_J^0$:

$$\chi = N\mu_B^2 [g_J^2 J(J+1)/3kT + \alpha_J] . \quad (3)$$

This is the case applicable to the rare earths and actinides in the temperature region of interest in this work. For the heavy actinides the

temperature independent part, α_J, is negligible compared to the temperature dependent term and will be neglected. The temperature dependent term has the Curie Law form,

$$\chi = \frac{C}{T} , \tag{4}$$

where $C = N\mu_B^2 g_J^2 J(J+1) = N\mu_{eff}^2$. The breakdown of Russell-Saunders coupling leads to a different value of g_J and thus μ_{eff}.

C. BREAKDOWN OF L-S COUPLING

In order to treat the breakdown of L-S coupling it is noted that the spin-orbit coupling which splits the L-S terms into J levels also couples together states of the same J but different L,S values. Since α_J and g_J above are determined by matrix elements of the type $\langle Jm|L_z + 2S_z|J'm'\rangle$, they do not couple states of different L and S. This means the perturbed α_J and g_J may be expressed as linear combinations of those for the different L,S terms. Thus the perturbed wavefunction, g_J, and α_J may be written in the form:

$$|\psi_J\rangle = \sum_{L,S} a_{L,S,J}|J,L,S\rangle \tag{5}$$

$$g_J = \sum_{L,S} a^2_{L,S,J}\, g_J(L,S) \tag{6}$$

$$\alpha_J = \sum_{L,S} a^2_{L,S,J}\, \alpha_J(L,S) , \tag{7}$$

where the $a_{L,S,J}$ are constants which determine the magnitude of the mixing of different L,S values to the unperturbed state.

The problem reduces to calculating the coefficients $a_{L,S,J}$ by diagonalizing the energy matrix in a perturbation approach. This method is outlined in a calculation of the susceptibility of Pu in the thesis of Dennis McWhan.[13]

Abraham, Judd, and Wickman[14] have calculated a value for g_J for Cm^{3+} of 1.913 using this method; while they have measured for g_J a value of 1.925 ± .002 using paramagnetic resonance of the Cm^{3+} ion in both ethylsulfate and trichloride crystals. This is to be compared with a calculated value of 2 for pure Russell-Saunders coupling for the $^8S_{3/2}$ ground state. For the rare earth counterpart Gd^{3+} a value of 1.991[15] has been determined from magnetic measurements.

In the metal several complications arise due to overlap of the atomic wavefunctions. First, the hybridization of the 5f atomic levels with the 6d7s levels may lead to fractional numbers of f electrons if one persists in describing the wavefunctions in atomic terms. A model proposed by Coqblin and Jullien[16] suggests that this may have a pronounced effect on the value of μ_{eff}. In this model, applied to the complete actinide series, the zero μ_{eff} values for the elements up to americium and a sudden "turn on" of magnetic moment for the elements beyond is explained in a qualitative manner in terms of hybridization. Also, the interaction between atoms whether due to direct exchange or to indirect exchange through RKKY oscillations in the conduction electrons leads to magnetic ordering at low temperatures and to a modified form of Curie law. This modified form:

$$\chi = \frac{C}{T + \Delta} , \tag{8}$$

is called the Curie-Weiss Law, where Δ is called the Weiss constant and C is the normal Curie constant.

CHAPTER III

MICROMAGNETIC SUSCEPTOMETER

A. OVERVIEW OF THE SYSTEM

A schematic of the susceptometer is shown in Figure 1. The magnetic moment of a sample is measured in a uniform magnetic field produced by the superconducting magnet. It is determined from the flux of the sample through the flux-sensing second derivative coils as measured with a Superconducting Quantum Interference Device (SQUID).[33] The flux is measured as a function of position in the coils as the sample is moved through the coils at a uniform velocity by the linear screw drive at the top of the cryostat.

The sample is embedded in a gold wire which is in turn encased in a quartz capillary as shown in Figure 2. One end of the gold wire is held by a copper chuck as shown in Figure 3, which is a detail of the part shown immersed in liquid helium in Figure 1. This chuck is held stationary with respect to the large copper cylinder at the bottom of the outer stainless steel tube by a beryllium-copper leaf spring. This provides thermal contact to the cylinder which serves as a thermal ballast and heater for the sample. Contained in the ballast are a carbon resistance heater, a carbon resistor thermometer, and a germanium resistance thermometer. Also a constantan wire heater is wound on its exterior. Sample motion through the flux-sensing second derivative coils is accomplished by moving the outer and inner stainless steel

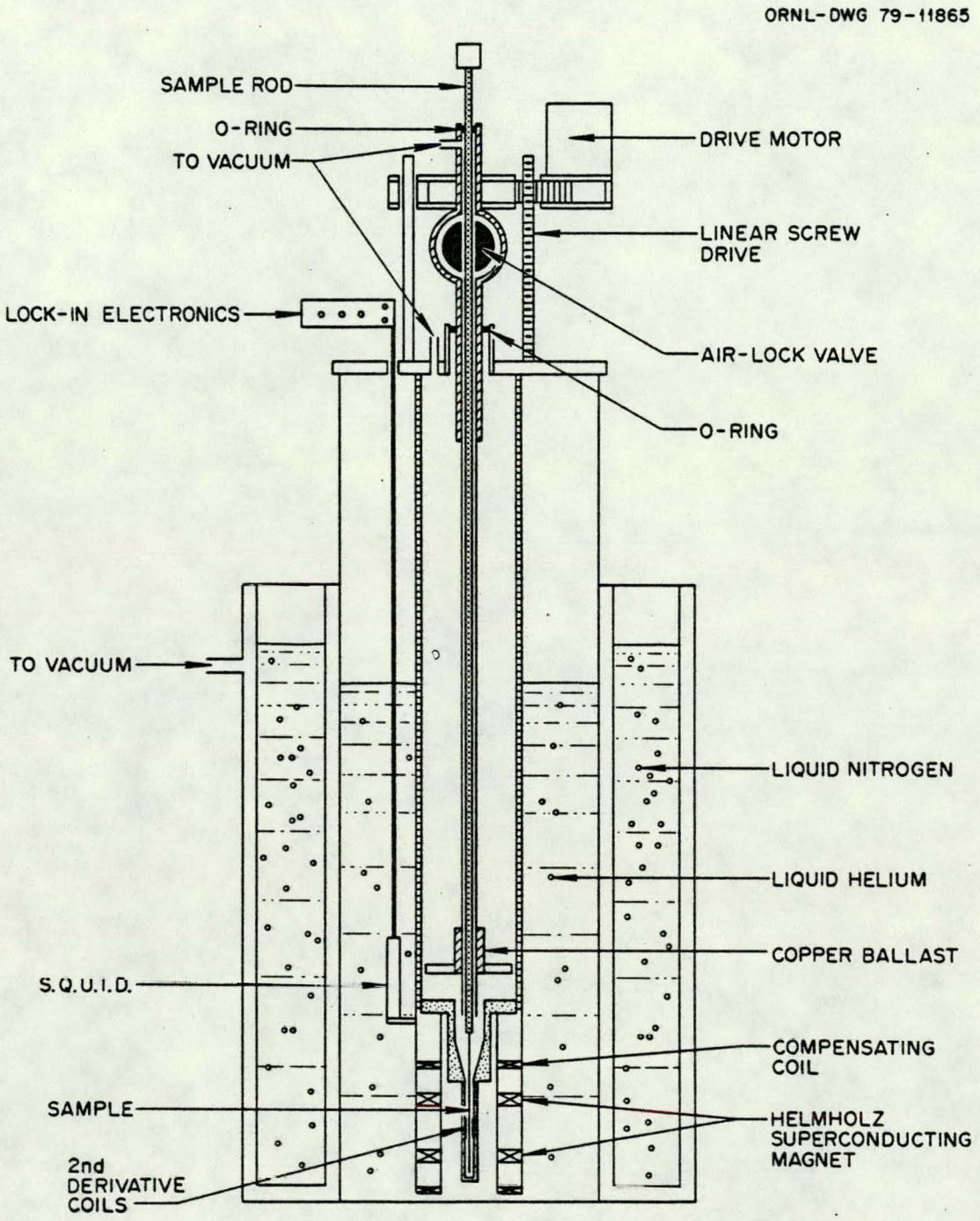

Figure 1. Overview of Susceptometer.

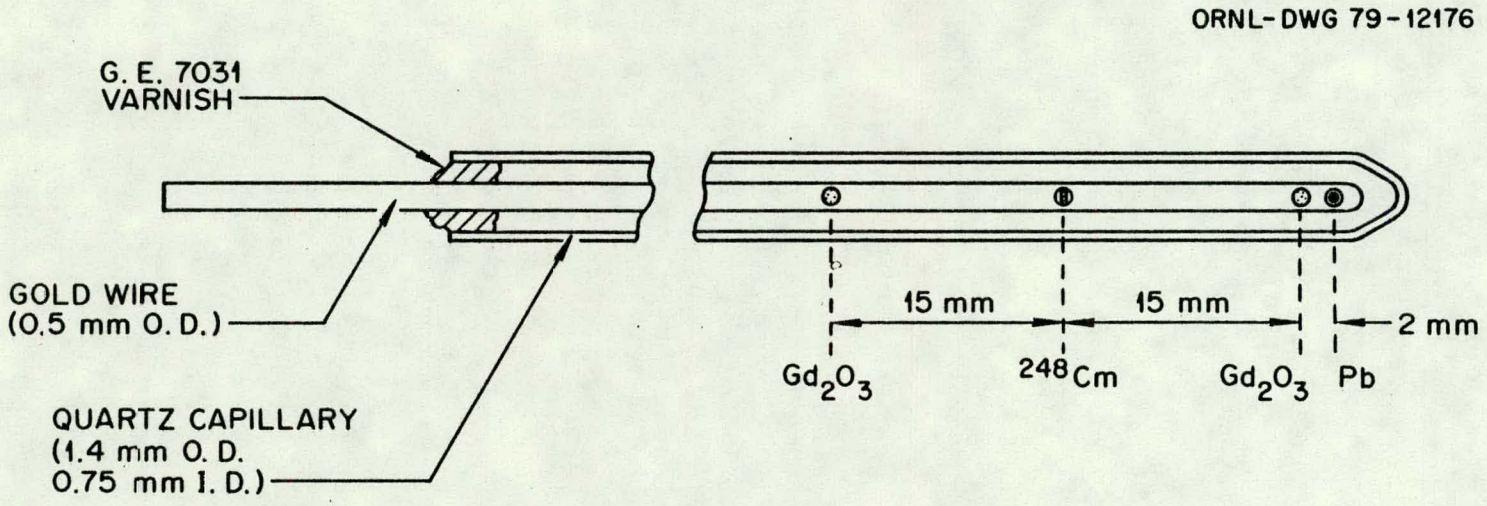

Figure 2. Sample Holder Configuration.

ORNL-DWG 79-11866

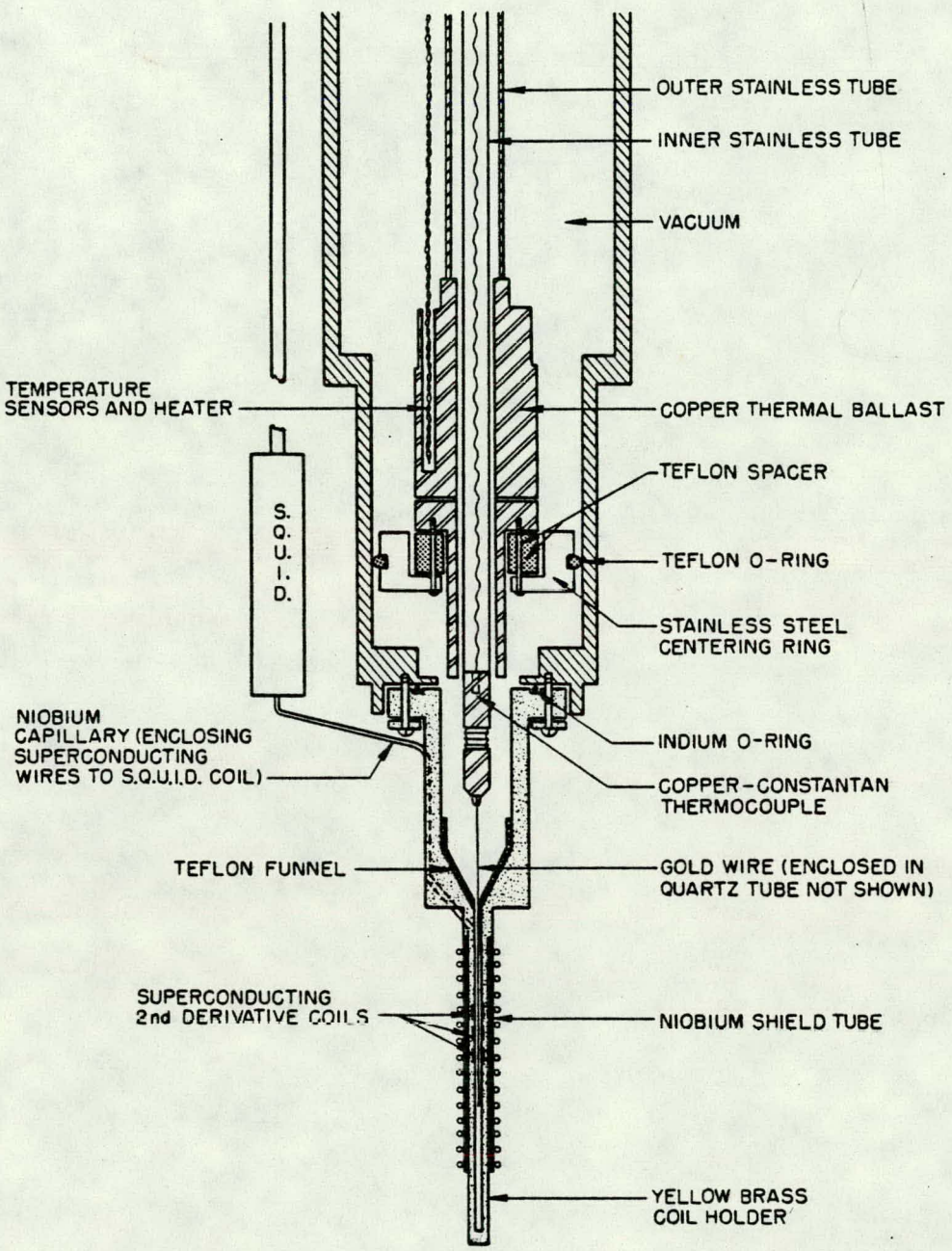

Figure 3. Detail of Low Temperature Part of Susceptometer.

tubes as a unit. The upper end of the outer stainless tube leaves the vacuum chamber through an O-ring seal as shown in Figure 1. Centering of the chuck is accomplished by the stainless steel centering ring in Figure 3. The ring is insulated from the copper ballast by a teflon ring with nylon screws and from the vacuum chamber walls by a split teflon O-ring, which also serves as a low temperature bearing. Any friction in the motion leads to vibration of the gold wire and sample and appears as magnetic noise on the signal. The necessity of insuring that the sample motion be very smooth led to this design. The inner stainless steel tube and chuck, which constitute the sample rod, may be removed and inserted during a run without losing vacuum in the vacuum chamber by using the airlock valve shown in Figure 1. The sample and chuck are inserted into the antechamber where the interior of the sample rod is evacuated. The ball valve is then opened and the chuck is lowered into place in the copper ballast. This gives the capability for multiple sample changes while the apparatus is cold and greatly increases the speed of operation.

B. FLUX MEASUREMENT

The susceptometer incorporates a commercially available[17] flux-sensing device of extreme sensitivity. This device, the SQUID, uses a Josephson junction[18] to sense DC flux level changes in an internal superconducting coil. A diagram of the device is shown in Figure 4. The Josephson junction, or weak link, is provided by the normal oxide layer on the screw tip that bridges the gap in the walls of the toroidal

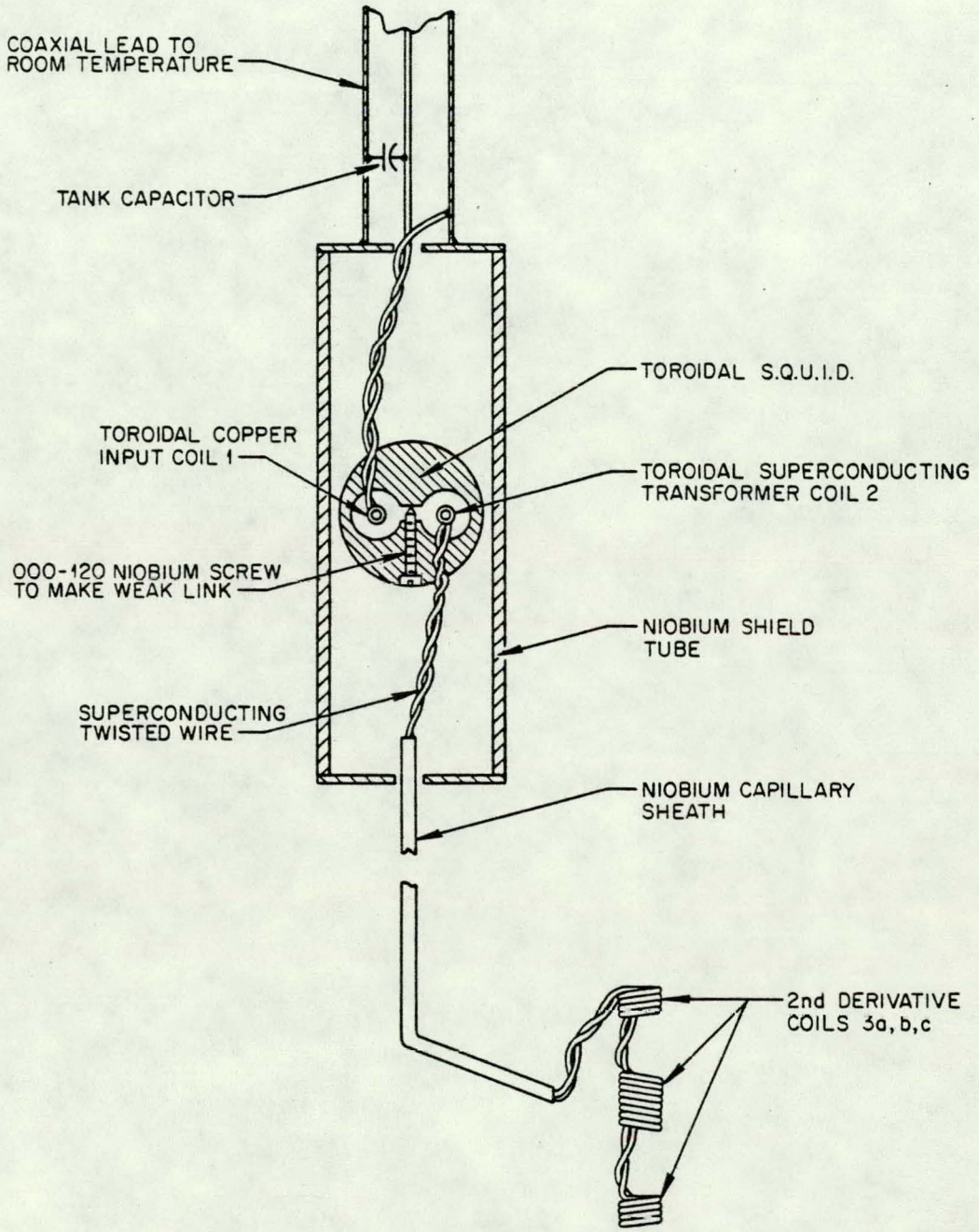

Figure 4. Cross Section of SQUID and Flux-Transformer.

superconducting cavity. Operation of this device is explained in Reference 19. The sensitivity of the device is limited by intrinsic noise to a value on the order of $4 \times 10^{-4}\ \phi_0$, where $\phi_0 = 2.07 \times 10^{-7}$ G-cm^2 is the quantum of flux and is less than one-millionth of the flux due to the earth's field through a coil with cross-sectional area of 1 cm^2.

The SQUID is operated in a "flux-locked loop" mode as a sensitive null detector for flux. DC flux is added to coil 1 in Figure 4 to null any external flux added to the SQUID cavity through coil 2 which is part of a superconducting flux transformer. The second derivative coils (3a, 3b, 3c) are the primary and coil 2 is the secondary of the transformer. A voltage proportional to the flux that must be added to the null coil is measured and calibrated in units of the flux quantum by allowing exactly one quantum to "slip," that is enter, into the SQUID cavity.

Since the flux through the area enclosed by a superconducting path must be constant, we have:

$$\Delta\phi_2 + \Delta\phi_3 + \Delta\phi_{leads} = 0 \ , \tag{9}$$

where $\Delta\phi_2$, $\Delta\phi_3$, and $\Delta\phi_{leads}$ are the changes in flux through coil 2, 3, and the twisted leads respectively due to an induced current Δi arising from a change in sample flux, $\Delta\phi_{sample}$. Also

$$\Delta\phi_2 = L_2\Delta i$$

$$\Delta\phi_3 = L_3\Delta i + \Delta\phi_{sample}$$

$$\Delta\phi_{squid} = M\Delta i \qquad (10)$$

$$\Delta\phi_{leads} = L_{leads}\,\Delta i \ ,$$

where $\Delta\phi_{squid}$ is the change in flux in the SQUID due to an induced current, Δi, in coil 2 and M is the mutual inductance between coil 2 and the SQUID cavity. L_2, L_3, and L_{leads} are the self-inductances of coils 1, 2 and the leads respectively. Thus $\Delta\phi_{squid}/\Delta\phi_{sample}$, which is the flux transfer ratio, f, of the transformer, is given by:

$$f = \Delta\phi_{squid}/\Delta\phi_{sample} = M/(L_2 + L_3 + L_{leads}) \ . \qquad (11)$$

It is difficult to measure the small DC inductances involved so a sample of known susceptibility was used to determine f directly. For these coils $f = 3.47 \times 10^{-3}$ as determined from experiments with a perfectly diamagnetic lead sphere as a calibrating agent.

C. SECOND DERIVATIVE COIL DESIGN

Since the SQUID is so sensitive to flux, the design of our sensing coils is chosen to maximize coupling to the sample flux but to minimize coupling to external magnetic fields. Because the sample is magnetized by a uniform applied field the coils should be relatively insensitive to changes in uniform fields. With the configuration shown in

Figure 4 (page 16) the coils are designed to be insensitive to changes in fields with constant first derivative as well as to changes in uniform fields and thus the name second derivative coils is used. The spacing between coils was chosen as small as possible without giving significant interference from sample flux through more than one coil at a time. Flux sensitivity can be shown to be maximized by choosing the inductance of the second derivative coils, L_3, and L_{leads} such that $L_2 = L_3 + L_{leads}$. L_2 is reported by the manufacturer to be 2.0 μH. By using a resonant LRC circuit, approximate measurement of the inductance $L_3 + L_{leads}$ was made as a function of number of turns of coil 3. From this it was concluded that the configuration shown in Figure 5 consisting of the two end coils with two layers of 8 turns each and the middle coil with two layers of 16 turns each wound in the opposite sense gave an approximate match to L_2 and thus maximized coupling to the sample flux.

D. SHIELD AND FLUX-TRAPPING TUBE

Since it is impossible to wind the coils perfectly, there is some sensitivity to uniform field changes. For these coils an asymmetry of 1554 ϕ_0/gauss was measured using the solenoid in Figure 5 to produce a uniform field. Figure 5 is a detail of the second derivative coil area of Figure 3 (page 14). This sensitivity makes it necessary to shield the coils by using a superconducting niobium cylinder[20] also shown in Figure 5. When a material becomes superconducting, currents flow within a thin layer at its surface to exclude any magnetic field from its interior as first observed by Meissner.[21] If the superconducting material

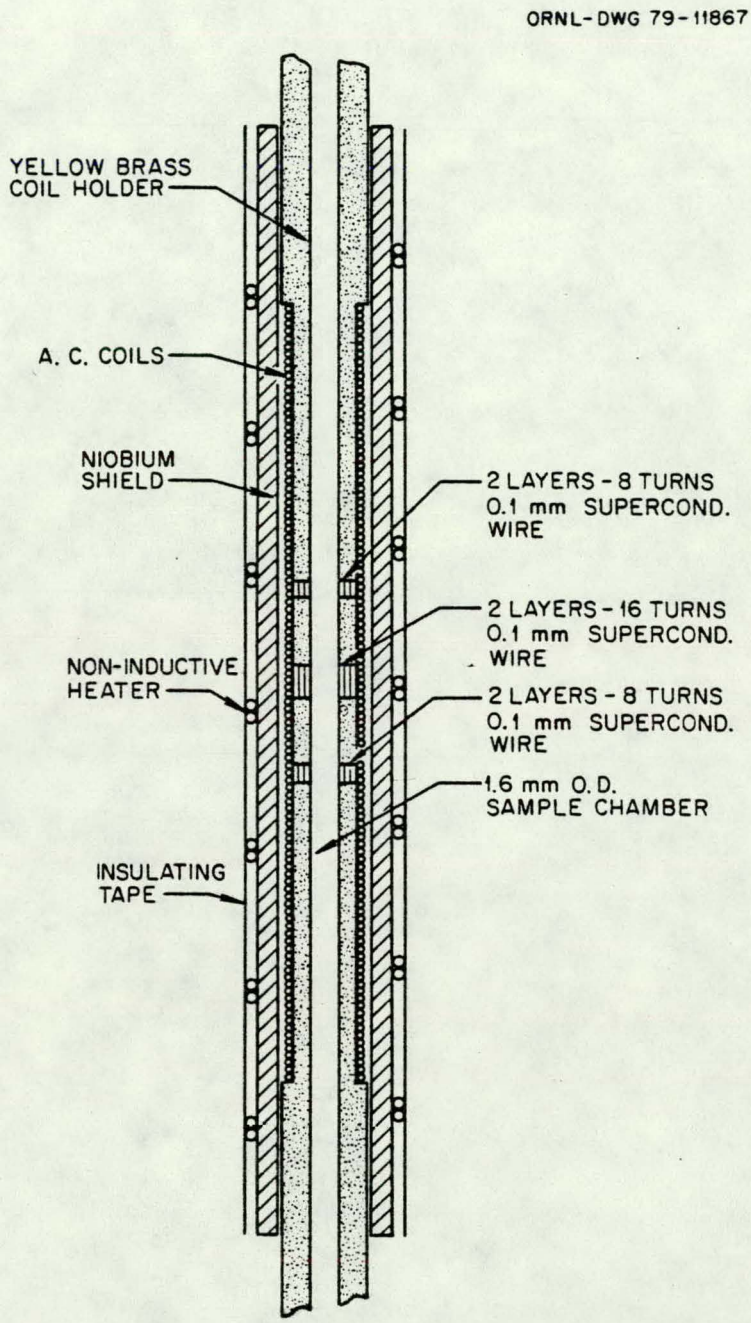

Figure 5. Second Derivative Coils and Flux-Trapping Tube.

is in the shape of a hollow cylinder the flux in its interior must remain constant, thus providing a good shield from changing external magnetic fields. Furthermore, if an external flux is present while the material is cooled to the superconducting state, the flux inside the cylinder will be trapped and constant in time. Such trapped fields have been found to be constant in time after many years of observation.[22] A field trapped in this manner is more uniform than can be produced with the magnet[23] and has a uniformity of 0.1% over the area of the coils. Thus the shield serves a dual purpose in that it traps a uniform field and shields from changing external fields. The shield has a non-inductive heater wound on its exterior which is insulated from contact with the liquid helium by a layer of masking tape. The heater is wound of 0.1 mm constantan wire and has a resistance of 500Ω at 4.2K. By applying 70 volts AC the temperature of the shield may be raised above its transition temperature while an external superconducting magnet is energized. When the current is turned off the shield quickly cools to trap the applied field.

The shielding ability of a cylindrical tube may be expressed as the ratio of the change in the interior field to the change in an external field. The shielding ratio, S, is much less for fields perpendicular to the shield axis than for fields parallel to the axis. Theoretically:[24]

$$S_{\perp} = e^{-1.84 \frac{d}{a}} \quad (1.5 \times 10^{-3} \text{ for our shield})$$

$$S_{\parallel} = e^{-3.83 \frac{d}{a}} \quad (5.2 \times 10^{-17} \text{ for our shield}) \,, \tag{12}$$

where a is the radius of the shield and d is the distance from the end to one of the end coils. We have measured an effective S of 1×10^{-8}. This was determined for our shield using the above asymmetry value of the second derivative coils as a measure of the average field at the coils. The superconducting magnet was energized while the shield was superconducting, and the fraction of this applied field seen at the coils was determined.

There was some concern over the size of the effect of a magnetic image of the sample due to the proximity of the shield. In a zero-order approximation the theoretical problem can be solved by treating the induced current distribution within the skin depth of the shield due to a sample in a single turn of the second derivative coils as a delta function at the same axial position as that of the sample as indicated in Figure 6. This approximation gives a correction factor

$$\frac{\Delta\phi_{sample}}{\phi_{sample}} = \frac{M}{L_0}\frac{b}{a} \simeq .01 \ , \tag{13}$$

where L_0 is the inductance of the shield segment of radius a. L_0 is on the order of 230×10^{-22} Henry assuming a skin depth of 500 Å. M is the mutual inductance between the shield segment and the single turn of the pickup coil of radius b. Fortunately, since the induced effect is linear, as is the case for the zero-order approximation, it is eliminated by calibrating the coils with a sample of known susceptibility.

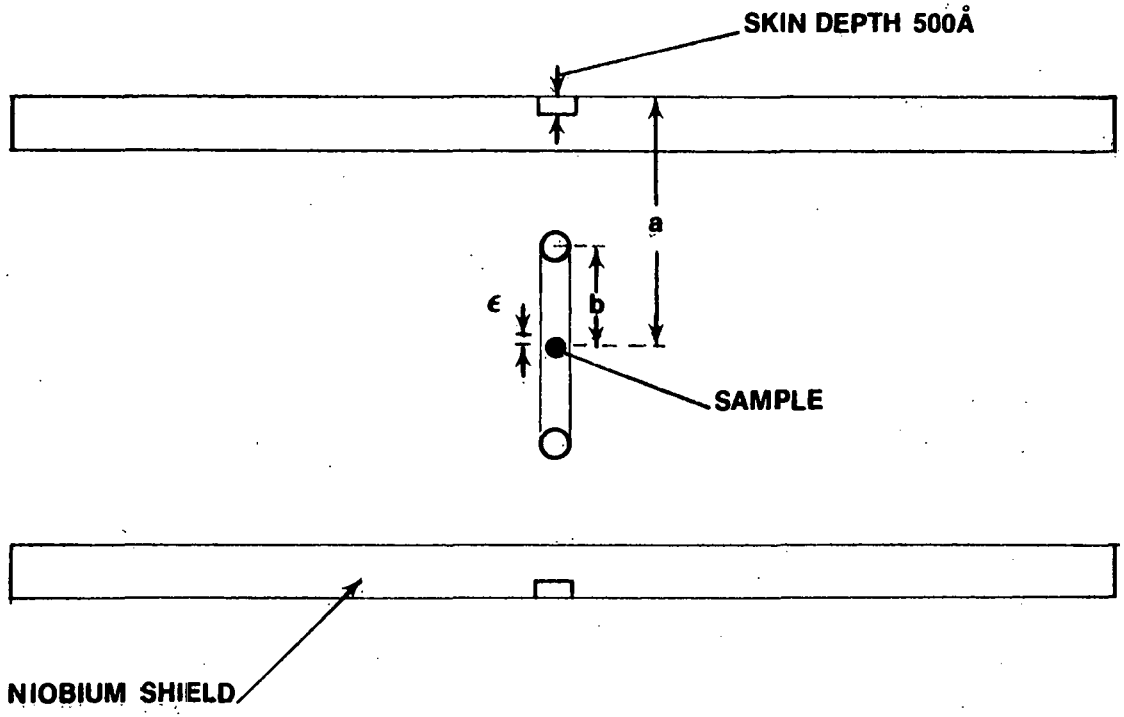

Figure 6. Diagram Illustrating the Zero Order Approximation to the Image Problem.

E. SUPERCONDUCTING MAGNET

The magnet which provides the applied field consists of a pair of Helmholtz coils with opposing trim coils on the ends to reduce the field in near proximity to the magnet. This allows the SQUID to be much closer to the magnet when working at fields above the critical field of the niobium SQUID shield. The magnet is wound from superconducting wire and is capable of applied fields of 15 KG. It was calibrated using a Hall probe and over the region of the pickup coils has an average field per current of 148 ± 3 G/amp.

F. COIL HOLDER

Several problems were encountered in developing a form for holding the coils in place. Two requirements were placed on the coil holder material. First, it was required that it have a small susceptibility at 4.2 K to reduce any contributions to the magnetic noise due to a temperature dependent susceptibility of the coil holder coupled with slight changes in its temperature. Secondly, it was required to have a relatively high resistivity at 4.2 K to reduce magnetic noise from Johnson noise current-fluctuation-correlation[33] of the type that gives white noise in a resistor. This noise arises from magnetic fields due to correlation of the random electron motion. The correlation is reflected in eddy current decay times and thus is smaller for larger resistivity.

In the first attempt the coils and shield tube were embedded in a nonmagnetic, clear epoxy called Stycast 1266.[25] This was desirable

since no layer of material was needed between the inner coil radius and the quartz sample tube, as would be the case for a machined coilform. This gives the smallest possible radius for the coil and maximizes coupling to the sample. It was found that 0.16 cm is the minimum radius of bend of the 0.1 mm niobium wire for which the formvar insulation will remain intact. The coils were wound on a 0.16 cm rod which was removed after the epoxy had hardened. Unfortunately, the differential thermal contraction between the epoxy and the niobium wires and shield caused the coil wire to break after each complete thermal cycle.

Next, the coils were wound on a nonmagnetic stainless steel tube of O.D. 0.16 cm and wall thickness 0.13 mm. Both copper and tape spacers for the coils were tried. This configuration also led to breaks in the coils although they lasted through several thermal cycles. A possible cause was hypothesized to be the radial flexing of the thin-walled tube when a vacuum was pumped on its interior. Indeed the flux signal was significantly affected by small changes in pressure.

In order to increase the rigidity of the coil holder it was decided to machine the tube and spacers as a single piece with a tube of the same dimensions as the stainless steel tube. The metal chosen was yellow brass which meets the small susceptibility and large resistivity requirements on the coil holder material as well as being easy to machine. Yellow brass was chosen over normal machine shop brass, such as red brass, since it contains no lead. Brass containing lead is excluded because, from low temperature susceptibility measurements,[26] it appears that the lead resides in dispersed pockets

and is superconducting at 4.2 K. Indeed the largest part of the susceptibility is a temperature independent diamagnetism that can be accounted for by assuming it is due to that lead present with a susceptibility of $-1/4\pi$ (CGS).

The layers of the coils were separated from each other and the coil holder by a layer of cigarette paper and were held in place with GE 7031 varnish. Great care was taken to round any possible contact points between wire and coil holder. To increase rigidity a single-layer solenoid of 0.1 mm copper wire was wound on top of the second derivative coils. These coils are also used for generating AC fields for AC susceptibility measurements. This configuration is shown in Figures 3 and 5 (pages 14 and 20) and has lasted through many thermal cycles.

G. DATA ACQUISITION

The data for determining the moment of the sample and thus the susceptibility is in the form of signal flux, ϕ_{sig}, in flux quanta vs. position as determined from the motor-run time. The motor-run time is measured with a clock of millisecond accuracy and serves as an accurate measure of position since the sample is driven at constant velocity. A plot of a typical set of such data is shown in Figure 7. The data are taken and recorded in a digital form using a minicomputer (Tektronix model 4051) as indicated in Figure 8. There are two modes of operation. For small signals with time rate of change of flux, or slew rate, of less than 10^3 ϕ_0/sec, the signal flux is in

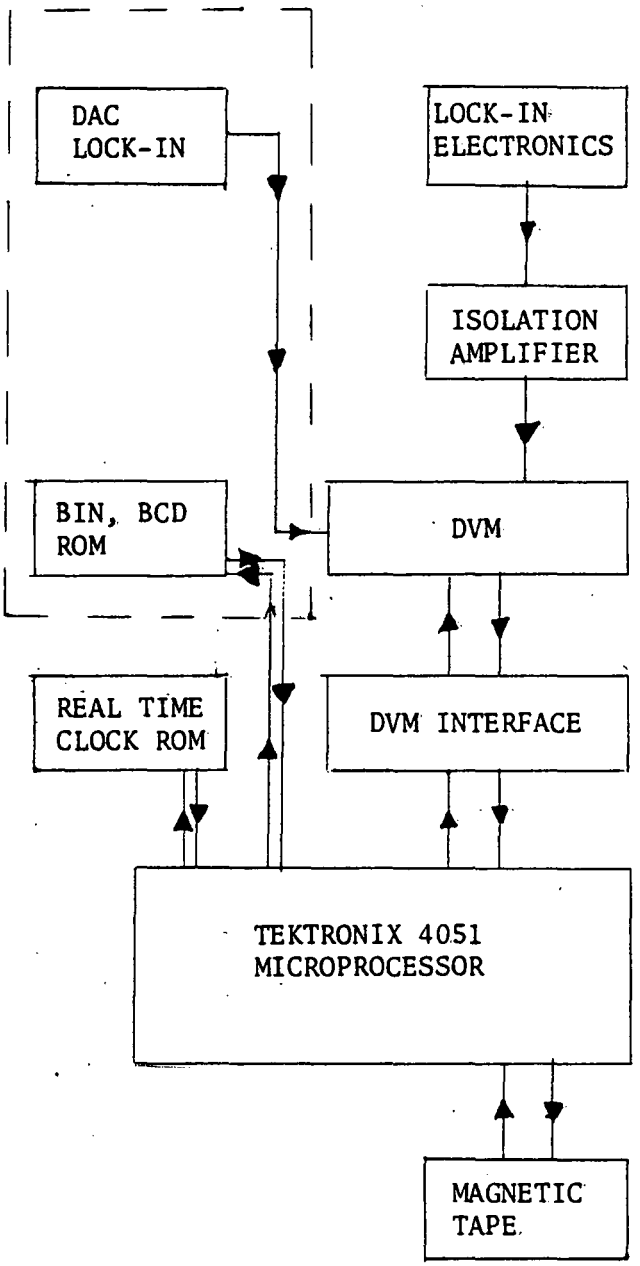

Figure 8. Data Acquisition System.

the form of a feedback voltage from the SHE model 202 lock-in electronics which has a measurement range of $10^3\ \phi_0$. This voltage is amplified and isolated from the measuring circuit by the isolation amplifier to avoid loading of the lock-in electronics and interference from the measuring circuits. The minicomputer requests a reading from the digital voltmeter (Dana model 5900) which digitizes the lock-in output and sends it to the computer by way of the BCD interface (Dana model 55). After the voltage is stored in memory the controller inputs the time of measurement from the real-time-clock ROM (Transera model 641-RTC). After a preset pause generated by the real time clock the process is repeated. On completion of the profile it may be plotted on the CRT for inspection and a hardcopy made. Then the digital data are recorded on a magnetic tape cartridge for further analysis at a later time. The second mode is used when the tracking rate of the feedback loop for the 202 electronics exceeds $10^3\ \phi_0$/sec. In this mode the 202 electronics are replaced by the electronics in the dotted box and consist of a SHE model DAC unit and interfacing. These electronics increase the tracking rate or slew rate to $10^4\ \phi_0$/sec and range to $10^5\ \phi_0$. The DAC output consists of the digital number of flux quanta and an analogue feedback voltage from 0 to 1 volt corresponding to the fractional number of quanta. The digital number is input to the controller through a binary-BCD rom pack (Transera model BCD) while the analogue signal is input through the DVM. The total number of flux quanta (integer plus fraction) is reconstructed in the program and stored with the time of measurement on magnetic tape as before. There is also the possibility

for using a computer controlled scanner (Hewlett-Packard model 3495-A) to consecutively input several different voltages as measured by the DVM to be stored with the time of measurement. The scanner consists of up to 20 relay activated channels to the DVM for different sources. The computer first closes a relay for a channel and then inputs the voltage reading on the DVM to the computer. In this mode the voltages for the sample and copper ballast thermocouple, copper ballast carbon and germanium resistors, and lock-in voltage may be recorded with the time. This completely automates the data taking process.

CHAPTER IV

SAMPLE HOLDER

A. CONSTRUCTION

The sample-holding configuration is indicated in Figure 2 (p. 13). A 0.25 mm diameter, 0.25 mm deep hole is hand-drilled in a 0.5 mm diameter, 99.92% pure gold wire. The wire is chemically etched in Aqua Regia for two to three minutes and rinsed in filtered, distilled water. The sample is cemented in the hole with varnish (GE-7031), and the wire is inserted in the 1.42 mm O.D., 0.75 mm I.D. fused quartz tube, which has been melted closed on one end. The quartz tube is washed in a 6M HCl solution followed by a filtered, distilled water rinse. It is sealed to the gold wire with varnish at the open end of the tube with about 10 mm of wire exposed for grasping in the copper chuck. This design was considered to provide an acceptable level of safety since it provides double containment for the radioactive sample.

B. MAGNETIC MEASUREMENTS ON AN EMPTY HOLDER

Gold wire was chosen since it has a relatively good thermal conductivity in the temperature range of measurement (4.2K to 300K). In addition, both it and the quartz tube meet the requirement of a small temperature independent susceptibility. This requirement is most important for the wire since we measure the "hole" as a pseudo-sample of a susceptibility equal to the negative of that of the wire. A series of

measurements were made on the empty sample holder as a function of field and temperature. In the first set of measurements an anomolously large signal was seen from the empty hole. On placing the "hole" in a field of greater than 100G and then returning to the earth's field the "hole" was permanently magnetized with a large moment. This initially cast doubt on the purity of the wire, but the profile of the end of the wire showed no such effect. Another possible explanation for this anomaly was that in drilling the hole with the high-speed-steel drill bit, iron particles were left behind and were not removed in the first wash consisting of a 6M HCl solution. It was found that after eating away the surface of the wire in Aqua Regia for two or three minutes the "hole" was magnetically clean. The "hole" showed a temperature independent susceptibility and from measurements on the profile of the end of the wire the value was determined to be -3.8×10^{-6} (CGS). The susceptibility of the quartz was also determined from its end profile, and a value of -1.6×10^{-6} (CGS) at 4.2K was determined.

C. WEIGHING AND LOADING OF SAMPLES

Weighing and loading of the samples into the sample holder was performed inside a specially constructed glove box containing an inert atmosphere and with an isolated filtered exhaust system. This was necessary as a safety precaution due to the high specific activity of the sample.

The sample was removed from a sealed quartz capillary containing an inert atmosphere as prepared in the metallic state. The sample is

weighed using a difference method by weighing an aluminum boat several times, weighing the sample plus boat several times and finally weighing the boat again several times. Statistics are then applied to the numbers which typically have a standard deviation of 0.2 μgram. The weighings are made using a Perkin-Elmer (model AD-2Z) balance with a claimed accuracy of 0.05 μgram using NBS Class M standard weights for calibration. Great care had to be taken to achieve the 0.2 μgram stated above. The biggest problem was due to static charges on the sample and balance due to lack of moisture in the inert atmosphere and charge buildup on the rubber gloves used for manipulation. By the use of alpha emitting sources under the pans of the balance and by care to remove charges on the gloves by grounding on the metal box walls, good results were achieved. Also care was taken to avoid magnetic contamination of the sample during the transfer process by using only a tungsten wire for picking it up. After weighing the sample is placed in its hole and coated with GE 7031 varnish to hold it in place and seal it from atmospheric contact. The quartz tube is then sealed into place also using the varnish.

CHAPTER V

DETERMINING THE SUSCEPTIBILITY FROM THE DATA

A. FLUX vs. POSITION FUNCTION

Four samples were placed in the wire, as shown in Figure 2, p. 13, and were measured simultaneously. The lead sample is for calibration, and the two Gd_2O_3 samples serve as thermometers. Results of displacing the wire through the coils are shown in Figures 7a and 7b, p. 27. It is noted that at 4.2K the lead and lower Gd_2O_3 sample signals interfere and must be mathematically deconvoluted, while above 7.2K the lead signal disappears (as it is no longer superconducting) and leaves only the Gd_2O_3 signal. Only one peak is seen for the upper Gd_2O_3 sample, but this is enough for analysis.

To determine the magnetic moment of a sample from the data, an expression must be derived for the total flux, Φ, through the second derivative coils in terms of the moment, μ, of the sample, which is assumed to approximate a point dipole. This is facilitated by making use of a form of the reciprocity theorem from electromagnetic theory. Assume the sample dipole is equivalent to a coil of radius ε and circulating current $\mu/\pi\varepsilon^2$. The flux, Φ, through this coil due to a current i in a turn of the second derivative coil of radius a is given by:

$$\Phi_1 = iM_{12} , \qquad (14)$$

where M_{12} is the mutual inductance as defined by this equation. Likewise, the flux through the turn of the second derivative coil due to the sample current is given by:

$$\Phi_2 = (\frac{\mu}{\pi\epsilon^2})M_{21} \ , \tag{15}$$

where M_{21} is the mutual inductance as defined by this equation. Reciprocity requires that $M_{12} = M_{21}$ and we thus obtain:

$$\Phi_2 = (\mu\Phi_1)/(\pi\epsilon^2 i) \ . \tag{16}$$

If ϵ is small enough we have:

$$\Phi_1 = B_0 \ \pi\epsilon^2 \ , \tag{17}$$

where B_0 is the axial component of the field due to the current i in this turn at the position of the sample. Thus we have:

$$\Phi_2 = \mu \ \frac{B_0}{i} \ , \tag{18}$$

and by summing over each turn of the second derivative coil we obtain:

$$\Phi = \mu \ \frac{B}{i} \ , \tag{19}$$

where Φ is the total sample flux and B is the total field at the sample due to the current i. An approximate expression for B/i is obtained by treating the second derivative coils as three sets of concentric

solenoids with inner radius a_1 and outer radius a_2. Each set has a width, W_i, and an axial position, L_i. B/i is given[27] in terms of these quantities as an expansion in even powers of the off-axis position by the expression:

$$\frac{B}{i} = \sum_{i,j,k} \frac{2\pi n_0}{10} \frac{z_{ij}}{\rho_{ijk}} \left\{ 1 + \frac{3a_k^2 y^2}{4\rho_{ijk}^4} + \text{Higher Order Terms in } y^2 \right\} \qquad (20)$$

where

n_0 = turns per cm,

$z_{il} = z - L_i + W_i/2$,

$z_{i2} = W_i - z_{il}$,

$\rho_{ijk}^2 = z_{ij}^2 + a_k^2$,

y = off-axis distance,

z = axial position.

For an off-axis distance as large as $0.3a_1$, the y^2 term is only 1.8% of the zero-order term at the peak and the y^4 term provides a correction of only 0.39% and so it will be neglected. All dimensions are in centimeters and give $\frac{B}{i}$ in G/abamp.

B. COMPUTER FITTING OF DATA

The values for W_i, L_i, y, and a_1 were determined by a nonlinear least squares computer fit to a set of data of flux vs. position for one of the Gd_2O_3 samples with negligible background slope. The measured values were used as starting values and the quantities W_i, L_i, y, and a_1 were varied to minimize the sum of the squares with the above function

as the fitting function. During the fitting n_0 was fixed at 98.4 turns/cm since .102 mm O.D. wire was used, and a_2 was constrained such that $a_2 = a_1 + 0.15$ mm since there was a .05 mm layer of paper between the wire layers. The computer routine was a variation of Marquart's method[28] and was available as a standard program on the Tektronix 4051 minicomputer. The measured values and fitted values are given in Table II. A plot of the data points and fitted function is shown in Figure 9. Figure 10 shows a plot of the residuals, i.e., the difference between the data and the fitted function, for the case where y^2 is fixed at zero. This is to be compared with Figure 11 which is a theoretical plot for the y^2 term using the fitted parameters.

C. DETERMINATION OF SUSCEPTIBILITY

To determine the susceptibility these computer-determined parameters were used in expression (20) for determining the peak-to-peak asymmetry of the second derivative coils. This is defined as the ratio of the left peak-to-peak value, f_1, divided by the right peak-to-peak value f_2. It was determined that $f_1/f_2 = 1.0077$. The peak values are determined by fitting a parabola to the three points nearest the peak and then determining the extremum of the parabola. Any profile with an asymmetry differing from this is said to have a sloping background and thus the peak-to-peak values are altered as given by:

$$f_1' = f_1 - m\Delta z_1 \,, \qquad f_2' = f_2 + m\Delta z_2 \,, \tag{21}$$

where f_1' and f_2' are the altered left and right peak-to-peak values

TABLE II

COMPARISON OF MEASURED COIL DIMENSIONS AND THOSE DETERMINED BY COMPUTER FIT TO DATA

Quantity (Eq. 20)	Measured Value (mm)	Fitted Value (mm)
a_1	.895	.750
a_2	1.048	.900
W_1	.813	.880
W_2	1.626	1.738
W_3	.813	.901
L_2-L_1	4.394	4.478
L_3-L_2	4.394	4.445
y	--	.33

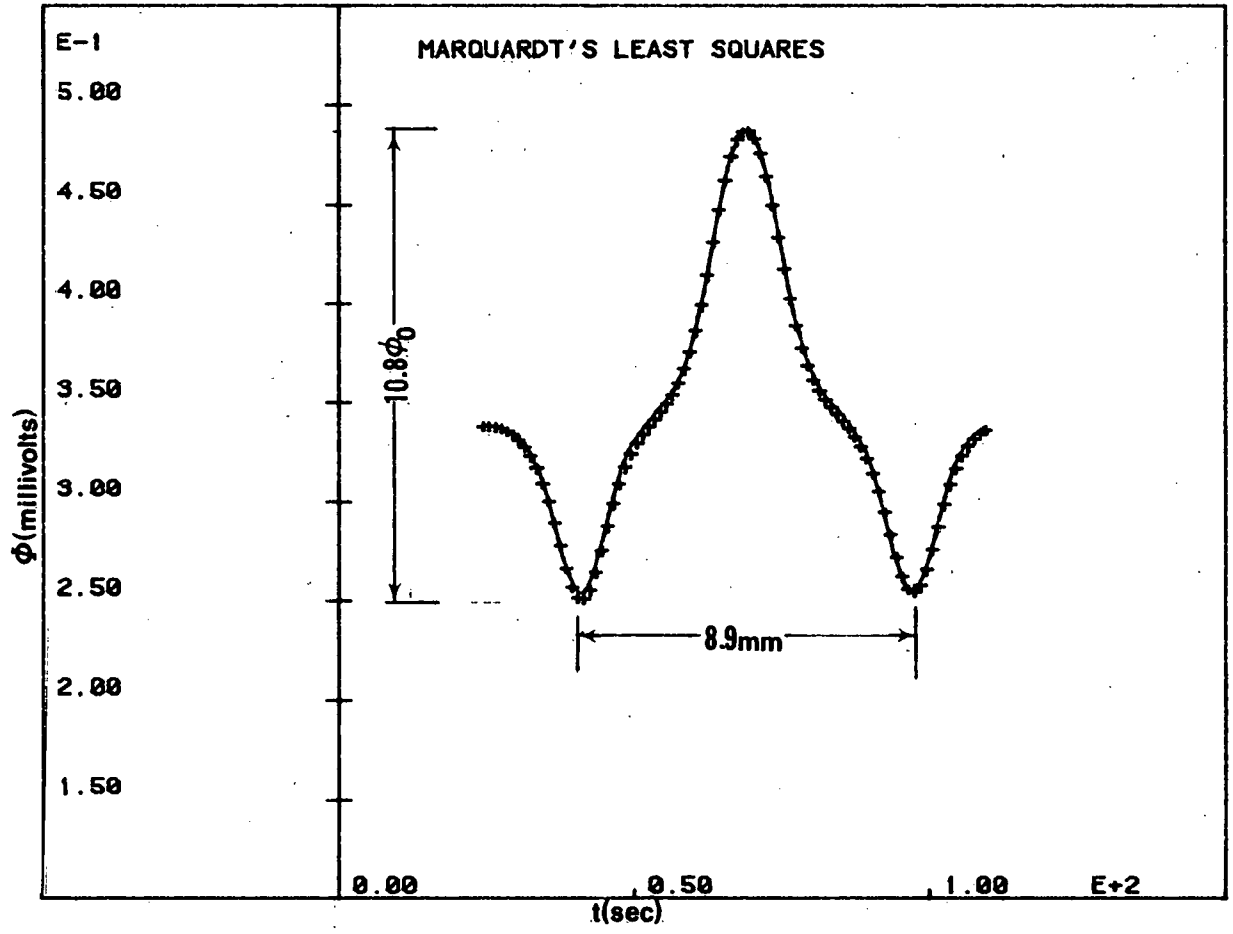

Figure 9. Computer Fit to the Sample Flux Profile.

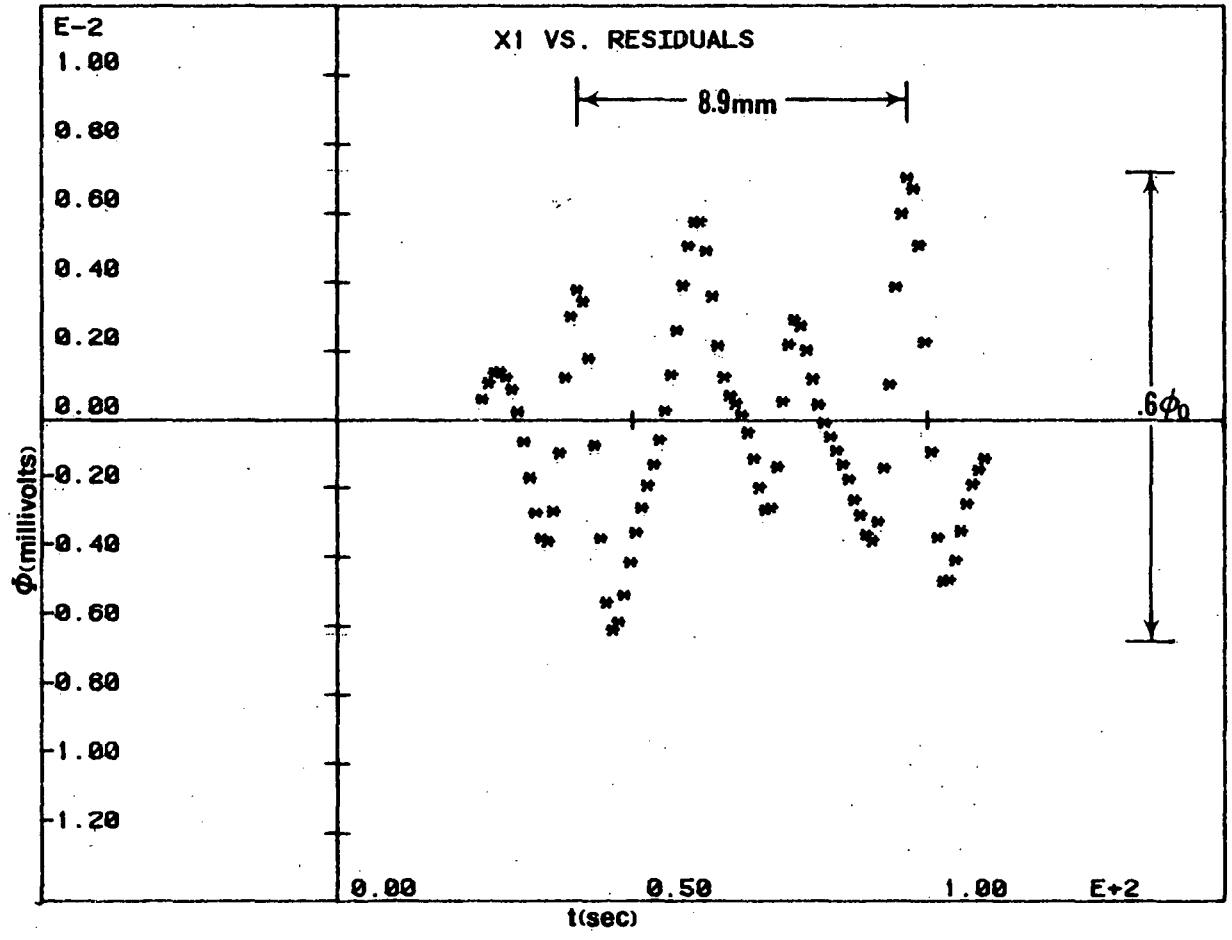

Figure 10. A Plot of the Difference between the Data of Figure 9 and a Computer Fit with the Off-Axis Distance Fixed at Zero.

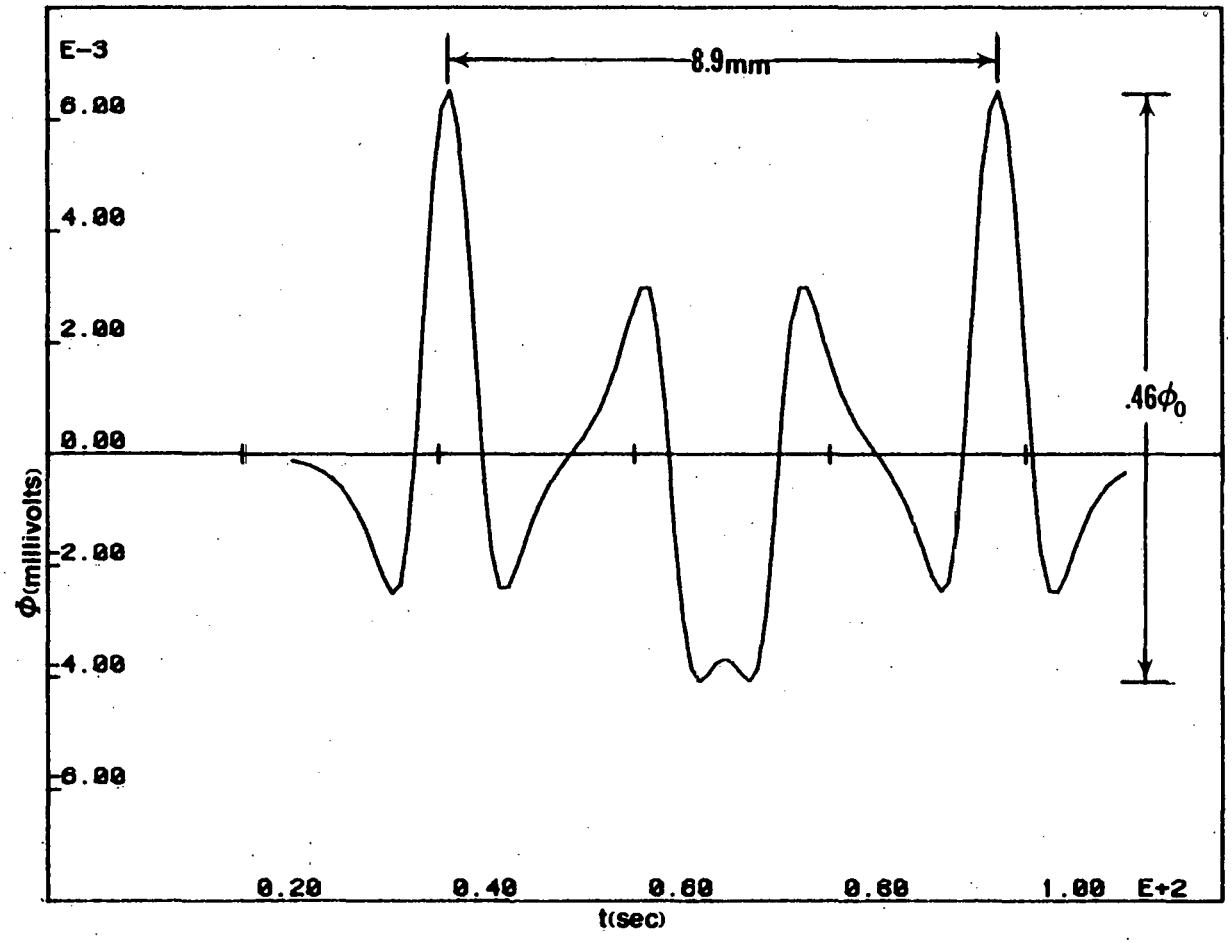

Figure 11. A Plot of the Theoretical Off-Axis Term for the Flux as a Function of Position for an Off-Axis Distance of .3 mm.

respectively, m is the slope of the background, and Δz_1 and Δz_2 are the left and right peak separations respectively. This slope is a sample holder effect probably due to taper in the gold wire or quartz and was seen in the measurements on the empty holder to be linear with field. The actual value, f_1, and the slope can be determined from the values f_1' and f_2' with values for Δz_1 and Δz_2 as determined for the coil spacing from the computer fit. f_1 is in this manner determined for the lead profile and the calibration quantity, $\alpha = f_1/\mu$, is calculated for the susceptometer. Here μ is the magnetic moment of the lead sample as calculated from its known susceptibility and volume (as determined from its mass). This quantity, α, is determined to be $47.159 \times 10^6\ \phi_0\ G^{-1}cm^{-2}$. The susceptibility of the unknown is then given by:

$$\chi = f_1/(\alpha V H_{applied}) \ , \tag{23}$$

where V is the volume of the sample as determined from its mass and density.

D. DECONVOLUTION

In order to obtain the profile for the lead at 4.2K, as stated above, the signal must be deconvoluted. This was accomplished using the nonlinear least squares fitting program with a fit to the profile of the form:

$$\Phi = \mu_1 \frac{B}{i}(0) + \mu_2 \frac{B}{i}(\Delta) \ , \tag{24}$$

where μ_1 and μ_2 are the magnetic moments of the two samples, $\frac{B}{i}(\Delta)$ is the expression in Equation (20) with $L_i = L_i + \Delta$ (Δ is the distance between the samples), and $\frac{B}{i}(0)$ is the unshifted expression. The variable parameters in the fit are μ_1, μ_2, Δ, baseline, and y. Figure 12 shows a plot of the data and computer fit as well as the deconvoluted profiles.

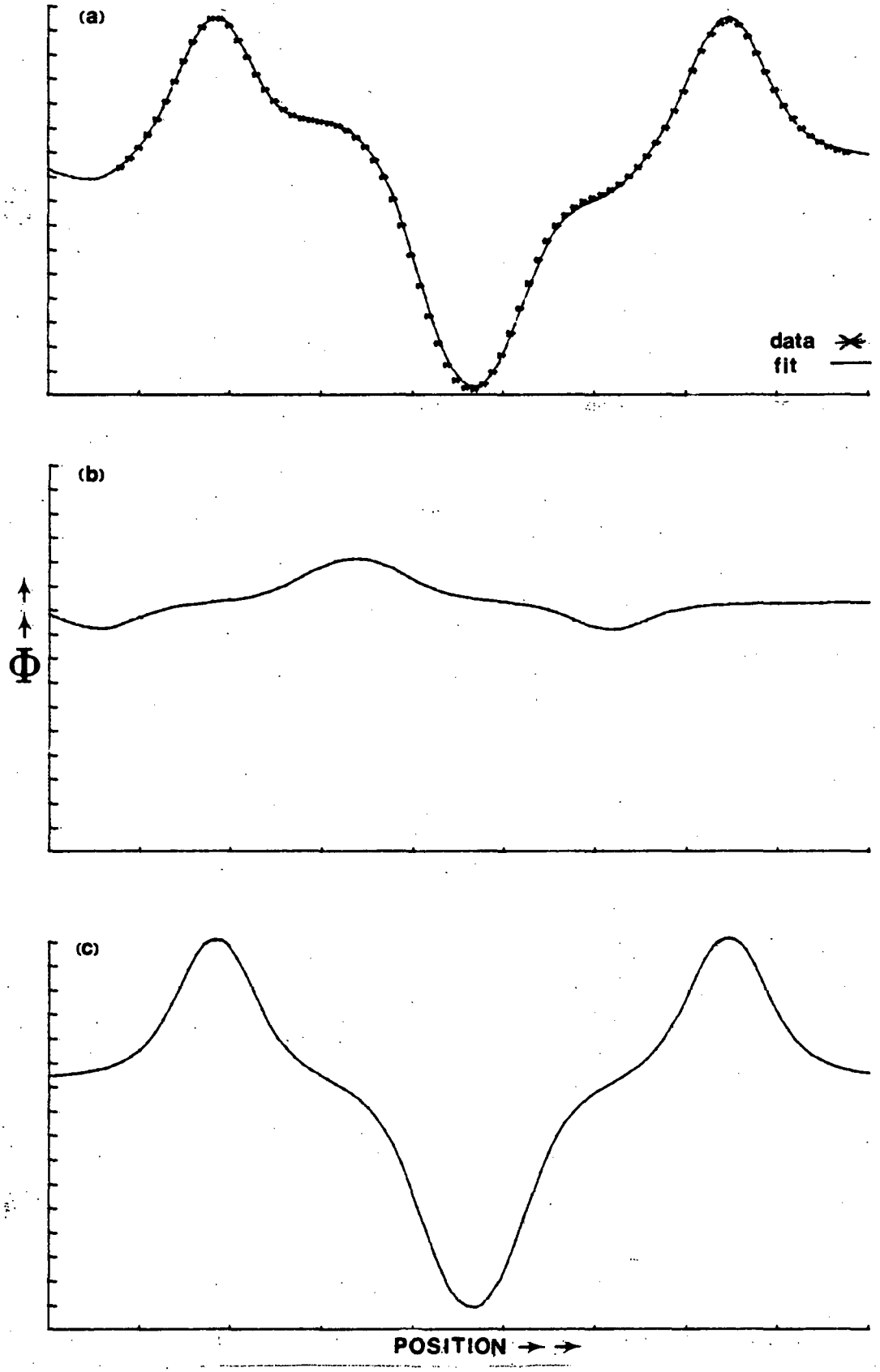

Figure 12. Deconvoluted Lead, Gd_2O_3 Flux Profiles.

CHAPTER VI

CALIBRATION OF THE SUSCEPTOMETER WITH A LEAD SPHERE

A. DEMAGNETIZING FACTOR

In order to calibrate the susceptometer, a spherical lead sample was included in the wire with each unknown sample to be measured as shown in Figure 2 (p. 13). Since lead is superconducting at temperatures less than 7.2K (in zero field) it will have a susceptibility of $-1/4\pi$. Due to the demagnetizing field of the sample the quantity that is measured is an effective χ,

$$\chi_{eff} = \frac{M}{H_{applied}} = \frac{\chi}{1 - D\chi} \tag{25}$$

where $\chi = M/H$, M is the magnetization, $H_{applied}$ is the applied field, H is the applied plus demagnetizing fields, and D is the demagnetizing factor which depends on the shape of the sample. For a sphere $D = 4\pi/3$. For samples with small susceptibility this correction is negligible but for lead D must be known to a relatively high degree of accuracy. On the other hand, the large χ of superconducting lead is desirable for a calibrating standard in order to increase the signal-to-noise ratio. Thus for the lead the magnetic moment is given by:

$$\mu = \chi VH = \chi_{eff}\, VH_{applied} ,$$

$$= \frac{3}{2}\left(\frac{-1}{4\pi}\right) VH_{applied} . \tag{26}$$

The calibrating spheres of lead are limited to a mass of less than 100 micrograms due to size restrictions.

B. PREPARATION OF SPHERES

It was attempted to make a good sphere by taking advantage of the surface tension of molten lead to do the shaping. To prepare a spherical sample a small splatter of 99.995% chemically pure lead was cleaned of its oxide layer in a 6M-HCl solution. It was then rinsed in filtered, distilled water and heated above its melting point in the flame of a torch on a flat carbon surface. By this method very shiny particles with an average deviation in radius of less than 1% could be produced. Evidently the carbon acts as a getter for oxygen as the sample cools in the atmosphere, thus preventing oxidation. Even if an oxide layer forms of thickness on the order of 50 Å this is only 10^{-5} of the total volume and provides a negligible correction.

C. SPHERICITY

A plot of the magnetic moment of the lead versus that of the Gd_2O_3 sample as the field is varied between 0G and 600G at 4.2K is shown in Figure 13. The moments of each are determined by deconvoluting their interfering profiles. The Gd_2O_3 moment is used as a linear measure of trapped field instead of the magnet current in order to eliminate any error due to irreproducibility of the trapping process. For fields between zero gauss and two-thirds of the critical field for lead (540.2 ± .1G at 4.2[30]) the lead moment is linear with the

applied field. Above 360.1 G the field penetrates the lead sphere, and an intermediate state consisting of normal and superconducting laminar regions develops.[29] As the fraction of normal region increases, the moment decreases linearly with field and finally reaches zero at the critical field. By fitting straight lines to the data points before and after the maximum moment for the lead sample a measure of its sphericity can be obtained. The ratio of the line segment $\overline{AB}$ to $\overline{AC}$ of Figure 13 should be 2/3 for a perfect sphere. The value obtained from the intersecting straight lines is 0.698.

D. DETERMINATION OF THE MAGNETIC FIELD WITH THE SPHERE

A linear least squares fit to the Gd_2O_3 moment versus magnet current is used to determine the current corresponding to the Gd_2O_3 moment value at the intersection point B of Figure 13. Since the field at this point must correspond to 360.1 G, a value for $H_{applied}/i$ of 141.9 G/A (±0.12%) has been determined.

The Gd_2O_3 moment provides the most accurate measure of trapped field. The ratio of the moment to the field is determined from the known field at the intersection point B in Figure 13. The field for each profile is then determined from the Gd_2O_3 moment. This measure of the trapped field eliminates flux rearrangement effects in the trapping process that could cause an error if the magnet current is used to determine the field. The discrepancy between the value of 148 G/A as measured for the magnet with a Hall probe and the value of 141.9 G/A is probably accounted for by this flux rearrangement on trapping.

CHAPTER VII

THERMOMETRY

A. COPPER-CONSTANTAN THERMOCOUPLE

Our primary temperature sensor was a copper-constantan thermocouple soldered in an indentation in the back of the copper chuck as indicated in Figure 3, p. 14. The reference junction was in a liquid nitrogen bath. The temperature was determined as follows: The NBS tables were reproduced to an accuracy of 0.1°C using the expression:

$$\text{EMF} = \begin{cases} A_1 T + B_1 T^2 + C_1 T^3 \ , & T < -195.6°C \ , \\ \\ A_2 T + B_2 T^2 + C_2 T^3 \ , & T > 195.6°C \ . \end{cases} \tag{27}$$

$A_{1,2}$, $B_{1,2}$, and $C_{1,2}$ were determined by requiring the expression to give the table EMF at three equally spaced temperatures in each interval. The table EMF value at a particular temperature is obtained by applying a linear correction to the thermocouple EMF, measured with the DVM. This correction is determined for $T < -195.6°C$ by calibration at 4.2K in a liquid helium bath and at -195.6°C in a liquid nitrogen bath. The correction for $T > -195.6°C$ is obtained by calibration at -195.6°C in the liquid nitrogen bath and at 0°C in an ice-water bath. The temperature is determined by inverting the appropriate expression above using the corrected potential value.

B. Gd_2O_3: A MAGNETIC THERMOMETER

Since the copper-constantan thermocouple is not as sensitive below 70K as it is above 70K, it was decided to use the temperature dependence of the susceptibility of Gd_2O_3 as a secondary temperature sensor. The oxide of gadolinium was chosen since it has been well measured and its inverse susceptibility is reported to be linear in temperature—even down to 4.2K.[30] This is thought to occur for two reasons: First, its atomic radius is small enough that the exchange interactions with near neighbors are negligible which means no magnetic ordering occurs in this temperature range. Secondly, since it has an f^7 electronic configuration, its ground state is an L = 0 state. This means that there is negligible crystal field splitting of the ground state which would lead to a temperature dependent effective magnetic moment in Equation (8). W. F. Giaque and J. W. Stout[30] report the values $\mu_{eff} = 7.898\ \mu_B$ and $\Delta = 15.5K$ for Gd_2O_3 in the temperature range from 30K to 298K. Below 30K Δ gradually increased to a value of 16.36K at 4.2K.

Figure 14 shows a plot of $1/\Phi_{signal}$ versus thermocouple temperature, T_c, with a least squares fit straight line for the data points between 15K and 90K. Here Φ_{signal} is the peak-to-peak value of the Gd_2O_3 profile. The intercept of the line is at -12.5K compared to the reported -15.5K and indicates an average shift of 3.0K between sample and thermocouple or a different Δ value due to impurities. The mean deviation of $1/\Phi_{signal}$ from the fit line is $9.7 \times 10^{-5}\ \phi_0^{-1}$ and corresponds to an effective temperature deviation of 0.2K. The maximum deviation from

THIS PAGE

WAS INTENTIONALLY

LEFT BLANK

the line corresponds to a temperature of 0.6K. This deviation is roughly equivalent to our level of temperature stability during the acquisition of a sample profile. Below 15K the data for $1/\Phi_{signal}$ are not accurately described by the fit to the higher temperature data with a maximum deviation of 1.5K.

For the first sample holder it was decided to put Gd_2O_3 samples on either side of the curium sample, as shown in Figure 2, p. 13, in order to see if any significant temperature gradients exist along the gold wire. The ratio of the signals from each of the Gd_2O_3 samples does not change significantly from that at 4.2K when exchange gas is in the sample chamber and thus indicated no measurable gradient over a 30 cm segment of the wire centered about the curium. A hole identical to the one described for curium was drilled in the gold wire for each of the Gd_2O_3 samples, which were a white powder of 99.9% purity. The powder was packed in the holes with a tungsten wire and was held in place using a light touch of dilute GE 7031 varnish.

CHAPTER VIII

RESULTS AND DISCUSSION

A. SENSITIVITY

By reducing the coil dimensions to give a diameter as near that of the sample as possible, more of the sample flux is coupled to the coils. In addition, by reducing the dimensions of the coil the magnitude of the magnetic noise is reduced. Magnetic noise may be due to: (1) susceptibility changes of nearby material due to temperature fluctuations with a period small compared to the time to take a profile, (2) vibration of coils in the trapped field, and (3) fluctuating fields due to correlation of the electron motion in nearby material (Johnson noise).

To a first approximation the signal flux Φ due to a point dipole of moment μ in an N turn coil of diameter d is given by:

$$\Phi_{signal} = fN \frac{4\pi\mu}{d} .$$

Here f is the flux transfer ratio defined in Eq. (11). In order to retain the matching condition ($L_2 = L_3 + L_{leads}$) as the coil diameter is reduced we must increase the number of turns. Since L_3 is approximately proportional to N^2d^2, Φ_{signal} is proportional to $1/d^2$. Also for values greater than the intrinsic noise of the SQUID ($10^{-4}\ \phi_0$) the magnetic noise is approximately proportional to d^2. For our noise level of $10^{-3}\ \phi_0$ this means the signal-to-noise ratio increases as $1/d^4$.

From preliminary tests with a 41.2 microgram sample of curium-248 we have determined a minimum detectable change in magnetic moment of 10^{-11} emu for the susceptometer. This may be compared to 3×10^{-9} emu for the best large-volume, superconducting susceptometer and represents an improvement of two orders of magnitude. This apparatus thus makes possible volume susceptibility measurements on a one microgram actinide sample in a 2000G field with a precision of better than 7.5×10^{-8} emu. By comparison Kanellakopulos[10] has used 24.8 mgm of ^{241}Am for measurement in an apparatus designed for actinides and obtained results to within 4.8×10^{-7} emu.

B. REPRODUCIBILITY AND ACCURACY

The precision of the susceptometer as a function of applied field at 4.2K was determined by comparing the peak-to-peak value for the combined lead-Gd_2O_3 signal for several profile runs, using the same magnet current to produce the trapped field. This comparison is expected to give a good estimate of error arising from such sources as hysterisis in the trapping of the field, flux rearrangement effects, changes in off-axis position of the sample, and spurious magnetic and electronic noise. For runs in the earth's field, corresponding to zero current, a standard deviation of 0.5% of the peak-to-peak signal was observed. For applied fields greater than about 10G the precision increased to a value better than that of the magnet current measurement. We have, therefore, chosen to use the lead plus Gd_2O_3 peak-to-peak signal as a field measure and observe the electronic and magnetic

noise error to be approximately 0.001 ϕ_0 at 20G fields. Since the curium signal is about 10 ϕ_0 in this field this corresponds to a precision of 0.02% for the curium sample moment measurement.

Accuracy determined from all sources of error to the susceptibility is approximately 0.8% and is predominantly caused by the ± 0.2 microgram limit of mass measurement of the lead and sample masses.

C. PRELIMINARY DETERMINATION OF CURIUM SUSCEPTIBILITY

Figures 15 and 16 show the experimental results for a 41.2 microgram sample of ^{248}Cm from the batch number 41278 and give the susceptibility as a function of temperature at applied fields of 0.45G and 20.9G respectively. It is clear from these figures that the character of the magnetic susceptibility is field dependent. In Figure 16 two magnetic transitions are seen: one in the range 77-78K, and one in the range 187-206K. In Figure 15 only one transition is clearly obvious, occurring in the range 70-80K, and only the one data point at 130K indicates a possible second transition. Due to the magnetic transitions there is serious doubt that we have taken any of the data at high enough temperature to fit to a true Curie-Weiss susceptibility law.

It seems likely that the 77K magnetic transition in the 20.9G temperature run is a true antiferromagnetic to paramagnetic transition. Evidence for this is based on the fact that the 4.2K value of χ is two-thirds of the value at 77K as it should be for an ideal polycrystalline antiferromagnetic sample.[31] For an ideal antiferromagnetic transition the susceptibility is different when measured with the field parallel

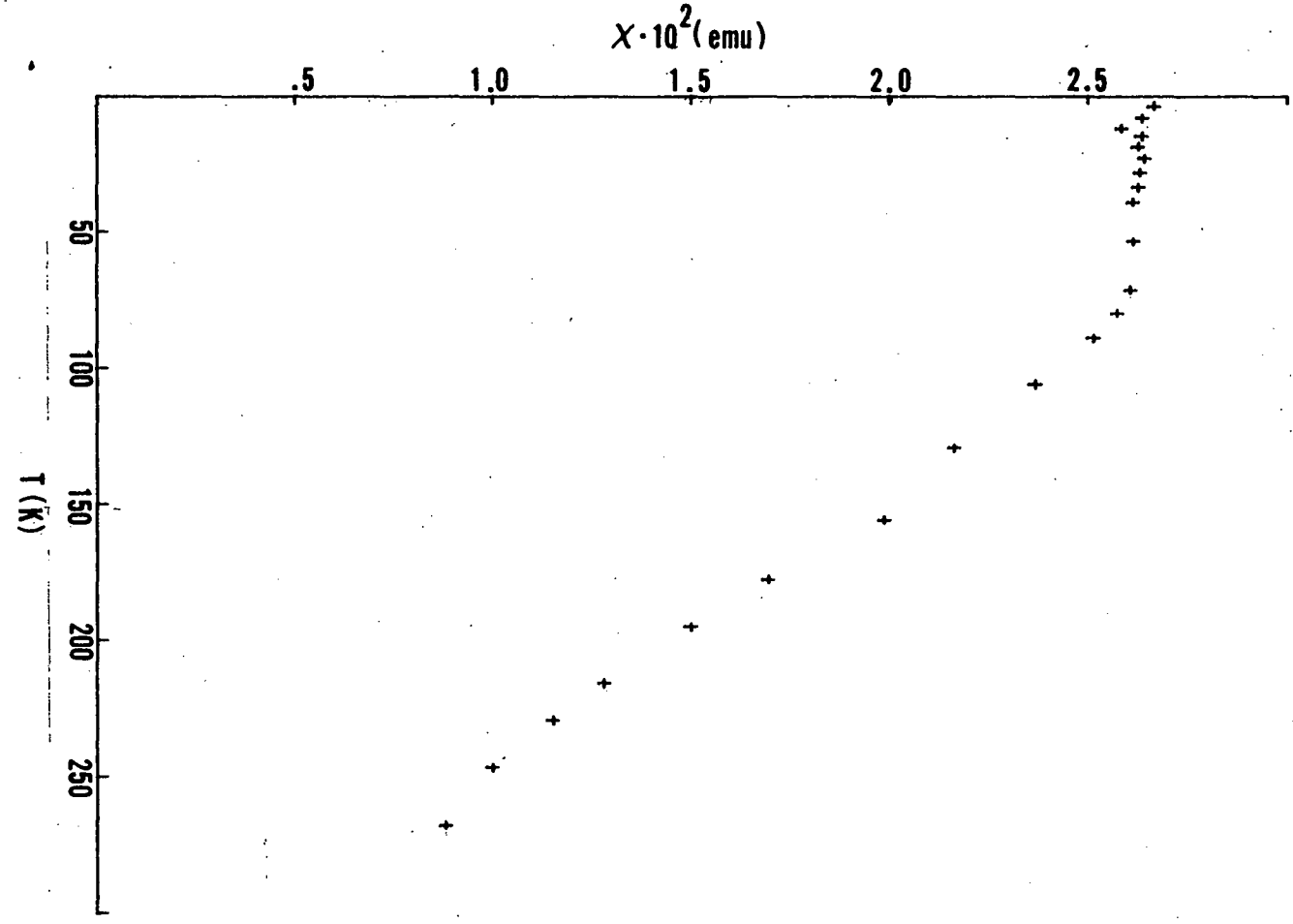

Figure 15. Susceptibility vs. Temperature for a 41.2 μgram Cm^{248} Sample at .45G.

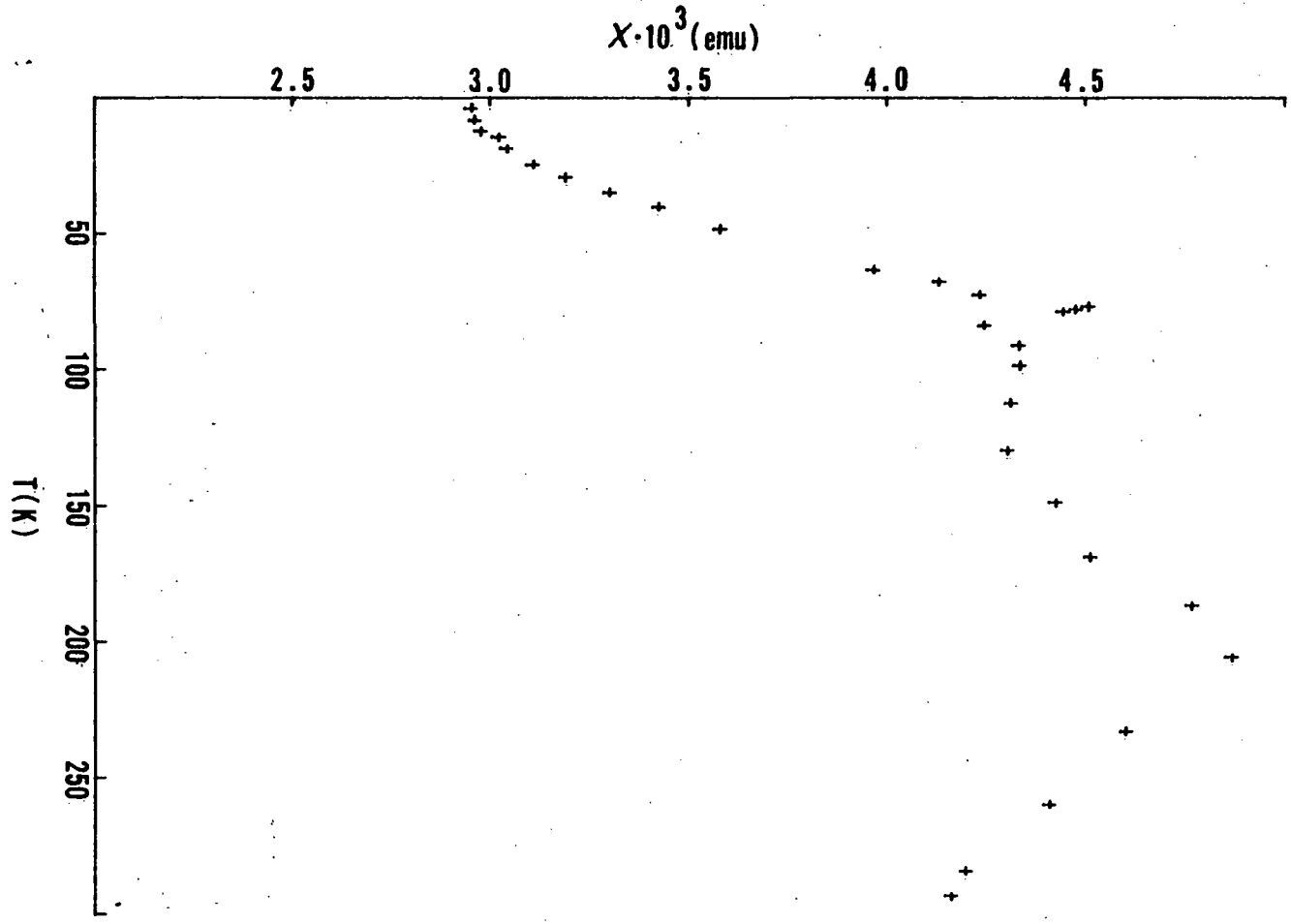

Figure 16. Susceptibility vs. Temperature for a 41.2 µgram Cm^{248} Sample at 20.9G.

and perpendicular to the alignment axis. The susceptibility measured parallel to the axis, $\chi_{\parallel}$, approaches zero at 0K and that measured perpendicular to the axis is constant for T less than T_N, the Neel temperature. For a polycrystalline sample one has an average over all possible orientations between the field and alignment axis. Since there are two equivalent perpendicular directions we have

$$\chi = \frac{1}{3}\chi_{\parallel} + \frac{2}{3}\chi_{\perp} \cdot \qquad (33)$$

This means that as T approaches 0K one should obtain $\chi(0K) = \frac{2}{3}\chi(T_N)$.

The temperature of this transition is slightly higher than that (52K) observed for ^{244}Cm.[10] It is possible that self-heating due to the higher rate of α-decay of ^{244}Cm could cause the average sample temperature to be warmer than indicated by the thermometer. It is also possible that the transition is field and/or radiation-damage dependent.

It should be noted that these results are only preliminary and serve to demonstrate the sensitivity and safe operation of the susceptometer with radioactive samples. Work is continuing on curium-248 from other preparations to determine if these results are influenced by impurities. The measurements will be repeated and extended to higher fields to determine accurately the correction for any permanent moment. Susceptibility measurements on large samples of very pure metallic elements like copper and silver show a slight field dependence at high fields (10-50 KG). This is generally attributed to a permanent moment due to ferromagnetic impurities. Such a permanent moment gives

a term proportional to 1/H in the susceptibility and can be corrected for by plotting χ versus 1/H and extrapolating to the value of χ at 1/H = 0. According to the mass spectrometric analysis in Table III there is less than 30 ppm of iron present in the original sample batch although more may have been introduced by handling with stainless steel forceps and cutting with a stainless steel knife. If this value is an upper limit on the amount of iron it could give a signal of only 0.5 ϕ_0 if due to saturated iron. This would be only a 4% correction to the 20.9G data and could not account for any of the observed structure.

D. CONCLUSION

In conclusion, a magnetic susceptometer with a sensitivity to small volume samples that makes possible measurements of microgram quantities of actinide metals has been constructed. This sensitivity has been demonstrated with preliminary measurements on a 41.2 microgram sample of Cm^{248}. In addition, novel methods for determining both the field and temperature of the actinide sample have been developed as a result of microscopic size limitations on any such conventional sensors to be placed in the microscopic sample region. The precision and accuracy of this device are such that the purity of the samples at present limit the accuracy of the results.

TABLE III

RESULTS OF Cm 41278 SPARK SOURCE MASS SPECTROLYSIS

Element	Abundance (Atomic ppm)
Ta	100
Mo	260
Fe	130
V	50
Ca	20
K	10
S	460
Si	90
Al	10
Na	10
Total	1140

REFERENCES

REFERENCES

1. M. Cerdonio, R. H. Wang, G. R. Rossman, and J. E. Mercereau, in "Proceedings of the Low Temperature Physics Conference," LT13 (1972), edited by E. Timmerhaus. Plenum, New York, NY, 1974.

2. Edward J. Cukauskas, Daniel A. Vincenot, and B. S. Deaver, Jr., Rev. Sci. Instrum. 45, 1 (1974).

3. J. S. Philo and W. M. Fairbank, Rev. Sci. Instrum. 48, 1529 (1977).

4. L. F. Bates, "Modern Magnetism," Chapter III, Syndks of The Cambridge University Press, New York, NY, 1961, p. 140.

5. Dennis Ken Fujita, Ph.D. Dissertation, University of California, Berkeley, 1969.

6. Allan R. Mackintosh, Physics Today 30, 23 (1977).

7. Robert B. Leighton, "Principles of Modern Physics," Chapter 8. McGraw-Hill, New York, NY, 1959, p. 259.

8. B. R. Judd and I. Lindgren, Phys. Rev. 122, 1802 (1961).

9. R. D. Baybarz, J. B. Knauer, and P. B. Orr, U.S. Atomic Energy Commission Document ORNL-4672 (1972).

10. B. Kanellakopulos, A. Blaise, J. M. Fournier, and W. Muller, Solid State Communications 17, 713-715 (1975).

11. W. T. Carnall and B. G. Wybourne, J. Chem. Phys. 40, 3428 (1964).

12. J. H. Van Vleck, "The Theory of Electric and Magnetic Susceptibilities." Oxford University Press, Oxford, England (1932).

13. Denis B. McWhan, Ph.D. Dissertation, University of California. Lawrence Radiation Laboratory Report UCRL-9695, The University of California, Berkeley, 1961.

14. Marvin Abraham, B. R. Judd, and H. H. Wickman, Phys. Rev. 130, 611 (1963).

15. C. A. Hutchison, B. R. Judd, and D. F. D. Pope, Proc. Phys. Soc. (London) B70, 514 (1957).

16. B. Coqblin, R. Jullien, and E. Galleani, Phys. Rev. B 6, 2139-2155 (1972).

17. S.H.E. Corporation, San Diego, CA.

18. Michael Tinkam, "Introduction to Superconductivity," Chapter 6. McGraw-Hill, New York, NY, 1975, pp. 192-229.

19. R. P. Giffard, R. A. Webb, and J. C. Wheatley, Journal of Low Temp. Phys. 6, 533 (1972).

20. B. S. Deaver, Jr., and W. S. Goree, Rev. Sci. Instrum. 38, 311 (1967).

21. W. Meissner and R. Ochsenfeld, Naturwissenshaften 21, 787 (1933).

22. Charles Kittel, "Introduction to Solid State Physics," 5th ed. John Wiley and Sons, New York, NY, 1976, pp. 382-383.

23. W. L. Williams, M. J. Stephen, and C. T. Lane, Physics Letters 9, 102 (1964).

24. Blas Cabrera and W. O. Hamilton in "The Science and Technology of Superconductivity," Vol. 2. Plenum Press, New York, 1973.

25. Marketed by Emerson and Cummings, Inc., Canton, MA.

26. G. L. Salinger and J. C. Wheatley, Rev. Sci. Instrum. 32, 872-874 (1961).

27. Herbert Bristol Dwight, "Electrical Coils and Conductors." McGraw-Hill, New York, NY, 1945, p. 289.

28. Tektronix Plot 50, "Statistics," Vol. 4. Tektronix, Beaverton, OR, 1977, p. 1-1.

29. Tinkam, pp. 97-98.

30. W. F. Giauque and J. W. Stout, Journal of Chem. Phys. 61, 1884 (1939).

31. Charles Kittel, p. 482.

32. R. E. Sarwinski, Cryogenics 17, 671 (1977).

33. J. B. Johnson, Phys. Rev. 32, 97 (1928).

34. D. L. Decker, D. E. Mapother, and R. W. Shaw, Phys. Rev. 112, 888 (1958).

VITA

Stanley Eugene Nave was born in [redacted]. He attended elementary schools in that city and was graduated from Elizabethton High School in June 1968. In September he entered East Tennessee State University in Johnson City, Tennessee. There he received a Bachelor of Science degree with a double major in physics and mathematics. The degree was conferred in June 1972 and in September he started a teaching assistantship at the University of Arizona, Tucson, Arizona, while pursuing his Doctor's degree.

After one year at that institution he returned to attend the University of Tennessee as a graduate teaching assistant and received a Master's degree in physics. At this point he was awarded a two-year fellowship by Oak Ridge Associated Universities to work on his doctoral dissertation at Oak Ridge National Laboratory. At the end of the two years his work continued with support from the University of Tennessee as a graduate research assistant. He received the Doctor of Philosophy degree with a major in physics in August 1979.

The author is a member of Sigma Pi Sigma, the Society for Physics Students, and the American Physical Society. After graduation he will continue his work at Oak Ridge National Laboratory while being employed as a postdoctoral student at the University of Tennessee.